Low Al-content n-type AlxGa1-xN layers with a high-electron-mobility grown by hot-wall metalorganic chemical vapor deposition

Vacuum 217 (2023) 112481

Contents lists available at ScienceDirect

Vacuum

journal homepage: www.elsevier.com/locate/vacuum

Low Al-content *n*-type $Al_xGa_{1-x}N$ layers with a high-electron-mobility grown by hot-wall metalorganic chemical vapor deposition

Vallery Stanishev [a,b], Nerijus Armakavicius [a,b], Daniela Gogova [a], Muhammad Nawaz [a,c], Niklas Rorsman [d], Plamen P. Paskov [a], Vanya Darakchieva [a,b,e,*]

[a] Center for III-Nitride Technology, C3NiT-Janzén, Department of Physics, Chemistry and Biology (IFM), Linköping University, 581 83 Linköping, Sweden
[b] THz Materials Analysis Center (TheMAC), Department of Physics, Chemistry and Biology (IFM), Linköping University, 58 183 Linköping, Sweden
[c] Hitachi Energy, 722 26 Vaesteras, Sweden
[d] Department of Microtechnology and Nanoscience, Chalmers University of Technology, SE-41296 Göteborg, Sweden
[e] Center for III-Nitride Technology, C3NiT-Janzén, Solid State Physics and NanoLund, Lund University, P.O. Box 118, 221 00 Lund, Sweden

ARTICLE INFO

Keywords:
AlGaN
MOCVD
GaN
Structural properties
Electrical properties

ABSTRACT

In this work, we demonstrate the capability of the hot-wall metalorganic chemical vapor deposition to deliver high-quality *n*-$Al_xGa_{1-x}N$ ($x = 0-0.12$, [Si] = 1×10^{17} cm^{-3}) epitaxial layers on 4H-SiC(0001). All layers are crack-free, with a very small root mean square roughness (0.13 – 0.25 nm), homogeneous distribution of Al over film thickness and a very low unintentional incorporation of oxygen at the detection limit of 5×10^{15} cm^{-3} and carbon of 2×10^{16} cm^{-3}. Edge type dislocations in the layers gradually increase with increasing Al content while screw dislocations only raise for x above 0.077. The room temperature electron mobility of the *n*-$Al_xGa_{1-x}N$ remain in the range of 400 – 470 $cm^2/(V.s)$ for Al contents between 0.05 and 0.077 resulting in comparable or higher Baliga figure of merit with respect to GaN, and hence demonstrating their suitability for implementation as drift layers in power device applications. Further increase in Al content is found to result in significant deterioration of the electrical properties.

1. Introduction

Ultrawide bandgap semiconductors such as diamond, AlN and Ga_2O_3 are attracting increasing research interest as promising materials for next generation power electronics [1,2]. Due to their high critical electric field (E_c) these materials can enable devices with lower resistance and lower capacitance as compared to their GaN and SiC counterparts. The critical electric field is directly proportional to the bandgap energy (E_g), $E_c \sim (E_g)^{2.5}$ [3]. In addition, the Baliga's figure-of-merit (BFOM) [4], which describes the relation between the material properties and the performance of power unipolar devices, is also proportional to E_c. Compared to SiC or GaN power devices, AlN allows thinner drift layer (×10) and efficient heat transport since the thermal conductivity of this material is superior [5] than that of conventional Si and even SiC/GaN power devices. Moreover, AlN is also used today in several commercial power modules for high power applications due to its superior thermal performance. $Al_xGa_{1-x}N$ ternary alloys offer the advantage to engineer the bandgap from 3.4 eV (GaN) to 6.0 eV (AlN). Thus, it is expected that $Al_xGa_{1-x}N$-based power devices can outperform GaN-based ones if other parameters of the $Al_xGa_{1-x}N$ active layers such as structural quality, electron concentration and mobility are kept similar to those of GaN. However, the latter present certain challenges posed by both practical implementations associated with growth and fundamental limitations.

For example, growth of $Al_xGa_{1-x}N$ layers by metalorganic chemical vapor deposition (MOCVD) is plagued by parasitic reactions in the gas phase between the Al precursor, trymethylaluminum (TMAl), and the group V precursor (NH_3) which causes poor growth efficiency, high dislocation density material and rough surface due to the generation of adducts as by-products of the parasitic reactions [6]. These effects become more likely to occur as the TMAl concentration in the vapor phase increases. Since the Al-N bond energy (2.88 eV) is higher than the Ga-N bond energy (2.24 eV) [7], the surface diffusion of adsorbed species will be impeded when increasing Al content [6]. This will result in a poor lateral growth with tendency to lead to three-dimensional growth mode as observed in rougher surface morphology at elevated Al compositions [8]. Due to limitations in surface diffusion, the growth of $Al_xGa_{1-x}N$ layers should be done at elevated temperatures as compared to the growth of GaN [9]. Growth at reduced pressure can be employed

* Corresponding author at: Center for III-Nitride Technology, C3NiT-Janzén, Department of Physics, Chemistry and Biology (IFM), Linköping University, 581 83 Linköping, Sweden.
E-mail address: vanya.darakchieva@liu.se (V. Darakchieva).

https://doi.org/10.1016/j.vacuum.2023.112481
Received 4 July 2023; Received in revised form 5 August 2023; Accepted 5 August 2023
Available online 9 August 2023

to reduce the probability of parasitic reactions and improve the crystal quality and surface morphology. However, challenges in achieving high *n*-type conductivity due to the increasing ionization energy of the Si donors with Al composition [10] and incorporation of compensating C acceptors remain [9]. Exploring low Al-content $Al_xGa_{1-x}N$ layers for potential use as drift layers in electronic devices presents some interesting opportunities as doping is readily achievable.

In order to realize low Al-content $Al_xGa_{1-x}N$ we employ hot-wall MOCVD approach, which has demonstrated some advantages with respect to the conventional cold-wall MOCVD systems in terms of more uniform temperature distribution and reduced strain gradients in the wafers. Furthermore, it proved beneficial for the generation of N and H radicals in the vapor phase, which improves the yield of the reactions leading to higher growth efficiency [11]. Recently, the growth of ultra-wide bandgap semiconductors by how-wall MOCVD such as β-Ga_2O_3 [12], AlN [13] and high-Al composition $Al_xGa_{1-x}N$ with well controlled doping [14] have been reported. Besides, the hot-wall MOCVD technique has demonstrated high quality GaN material with polarity and *p*-type doping control [15–17] as well as high purity homoepitaxial GaN with the smoothest surface morphology reported so far [18].

In this work, we aim to determine the threshold in Al content above which the crystal quality and electrical transport properties starts to deteriorate in order to determine the optimum x in *n*-type $Al_xGa_{1-x}N$ to be used as a drift layers in vertical power devices. For such application, a certain amount of Al is needed to increase the bandgap and thus the E_c and the BFOM of the potential device. However, the Al content should not be too high to facilitate formation of additional threading dislocation densities, rougher surface morphology and decrease of the electron mobility.

2. Experimental

A series of 700-nm-thick *n*-$Al_xGa_{1-x}N$ layers were grown in a horizontal hot-wall MOCVD reactor on semi-insulating 4H-SiC(0001) substrates at a reactor pressure of 100 mbar and a temperature of 1100 °C. The flows of the precursors trimethylgallium (TMGa) and NH_3 were kept constant at values of 2.2 ml/min and 2.0 l/min, respectively. Alloying with Al was achieved by varying the TMAl flow ranging from 0 to 0.05 ml/min and resulting in Al content x from 0 to 0.12 (Table 1). The doping with [Si] = 1×10^{17} cm^{-3} was realized by the use of a double hydrogen-diluted silane (SiH_4) source. Prior to the growth of *n*-$Al_xGa_{1-x}N$ layers, a 50-nm-thick AlN nucleation layer was grown at a pressure of 50 mbar, growth temperature of 1250 °C and V/III ratio of 460.

The surface topography of $Al_xGa_{1-x}N$ layers was studied by means of a Veeco Dimension 3100 Atomic Force Microscope (AFM) in a tapping operation mode. The layer thickness was determined by white light interferometry. The crystalline quality and lattice parameters were evaluated by high-resolution X-ray diffraction (HR-XRD) employing a PANalytical Empyrean diffractometer equipped with a four-bounce Ge(220) and a hybrid monochromator consisting of a parabolic X-ray mirror and two bounce Ge(220). The CuK_α radiation used has a wavelength λ = 1.5405974 Å. The lattice parameters and the strain were calculated as described previously [19,20].

The bandgap energies of the $Al_xGa_{1-x}N$ layers were determined from visible-near-ultraviolet spectroscopic ellipsometry (SE) data measured with a dual-rotating compensator ellipsometer (RC2 J.A. Woollam Co., Inc.). SE data were analyzed using the WVASE software (J.A. Woollam Co., Inc.) by fitting optical model spectra to the experimental data and employing a nonlinear regression algorithm. The optical model consisted of parameterized model dielectric functions to describe intra-band and band-to-band electronic transitions in the $Al_xGa_{1-x}N$ where the band gap absorption edge energy appears as a fitting parameter. The band gap energies were determined from the best-fit optical models as the energies of the band gap absorption edges. Cathodoluminescence (CL) spectroscopy was performed at room temperature with a Leo 1550 MonoCL2 system (Oxford Res. Instr.).

The free-electron concentration and mobility were determined by Hall-effect measurements performed at room temperature in Van der Pauw configuration with a Linseis CS1 instrument. For this purpose, Ni/Au (5 nm/ 250 nm) ohmic contacts were deposited by thermal evaporation and annealed at 450 °C in air. Capacitance–voltage (C–V) measurements with a mercury probe setup with a 4284 A LCR meter from Agilent are used to determine the net donor concentration.

The Al content, the Si doping concentration and the concentration of unintentional impurities (O, C and H) were obtained by secondary ion mass spectrometry (SIMS) through a depth profiling analysis. For this purpose, a special sample consisting of four consecutive 300-nm-thick Si-doped $Al_xGa_{1-x}N$ layers with different Al contents grown on semi-insulating SiC substrate, was fabricated. The Al content determined in the multi-layer sample versus TMAl to TMGa ratio was used to estimate the Al contents in the respective 700-nm-thick $Al_xGa_{1-x}N$ layer series. Selected samples were cross-checked with SIMS confirming the assignment.

3. Results and discussion

3.1. Crystal quality of layers

Representative AFM images, revealing the surface morphology of the *n*-GaN and *n*-$Al_xGa_{1-x}N$ epitaxial layers are shown in Fig. 1. The *n*-GaN layer exhibits an atomically flat surface with a root-mean-square roughness (RMS) of 0.12 nm over a 5×5 μm^2 scanning area. The surface roughness remains practically unaffected up to x = 0.065. In the *n*-$Al_xGa_{1-x}N$ layers with an Al content of x = 0.077 the RMS value increases to 0.17 nm and the highest RMS of 0.25 nm is observed for *n*-$Al_{0.12}Ga_{0.88}N$, where pits start appearing.

The dislocation densities were estimated using the rocking-curves of different symmetric and asymmetric GaN XRD peaks. Screw dislocations cause mosaicity by tilting the crystallites with distortions parallel to the *c*-direction. The tilt angle (α_c) was determined by employing the Williamson–Hall method. In this method, α_c represents the slope of the linear fit of the $\beta_\omega \sin(\theta)/\lambda$ versus $\sin(\theta)/\lambda$, where θ is the diffraction angle and β_ω is the full width at a half maximum (FWHM) of the GaN (0002), (0004) and (0006) rocking curves [21]. The screw dislocation density (D_S) was estimated by

$$D_S = \frac{\alpha_c^2}{4.35 b_c^2}, \quad (1)$$

where the magnitude of the Burgers vector along the *c*-axis is $|b_c|$ = 0.5185 nm.

Edge dislocations cause distortions parallel to the in-plane crystallographic directions, $< 11\bar{2}0 >$, i.e. a twist of the crystallites. The twist angle α_a was obtained from the plot of the FWHM of GaN (0002), $(10\bar{1}1)$, $(10\bar{1}2)$, $(10\bar{1}3)$, $(10\bar{1}4)$, and $(10\bar{1}5)$ versus the inclination angle from the surface normal [22]. In the fitting, the tilt angle obtained from the William–Hall plot was used as a fixed parameter. The edge dislocation density (D_E) was estimated by

$$D_E = \frac{\alpha_a^2}{4.35 b_a^2} \quad (2)$$

where $|b_a|$ = 0.3189 nm is the magnitude of the Burgers vector along the *a*-axis.

The densities of dislocations for all studied layers are shown in Table 1 and displayed in Fig. 2 as a function of Al content. As expected, the density of screw type dislocations is at least one order of magnitude lower as compared to the density of edge type dislocations in the GaN layer. This trend is preserved for all *n*-$Al_xGa_{1-x}N$ layers independent of Al content. The density of edge type dislocations increases notably with Al content. On the other hand, the screw dislocation densities remain similar to that of the GaN reference layer up to x = 0.065 and

Table 1
Summary of the structural and electrical properties of the layers with different Al content: Si concentration, screw (D_S) and edge (D_E) dislocation densities, net donor concentration, ($N_D - N_A$), electron concentration (n), mobility (μ) and bandgap energy (E_g). The estimated critical electric field (E_c) following [3] and BFOM relative to that of GaN following [4] are also shown.

Al content (%)	[Si] (cm^{-3})	D_S (cm^{-2})	D_E (cm^{-2})	$N_D - N_A$ (cm^{-3})	n (cm^{-3})	μ (cm^2/(V.s))	E_g (eV)	E_c (V/cm)	BFOM
0	8.4×10^{16}	3.6×10^{7}	4.9×10^{8}	7.7×10^{16}	3.9×10^{16}	541	3.44	3.8×10^{6}	1
2	1.2×10^{17}	2.3×10^{7}	8.8×10^{8}	–	6.3×10^{16}	517	3.48	3.9×10^{6}	1.04
3.1	8.5×10^{16}	4.8×10^{7}	1.0×10^{9}	6.7×10^{16}	4.3×10^{16}	376	3.51	4.0×10^{6}	0.81
5	1.0×10^{17}	1.4×10^{7}	6.7×10^{8}	–	7.1×10^{16}	468	3.54	4.1×10^{6}	1.05
6.5	1.2×10^{17}	2.9×10^{7}	7.8×10^{8}	8.5×10^{16}	4.9×10^{16}	396	3.56	4.2×10^{6}	0.95
7.7	1.2×10^{17}	7.9×10^{7}	1.2×10^{9}	6.3×10^{16}	4.4×10^{16}	407	3.58	4.3×10^{6}	1.02
12	1.0×10^{17}	9.4×10^{7}	1.2×10^{9}	5.8×10^{16}	5.0×10^{16}	194	3.66	4.5×10^{6}	0.57

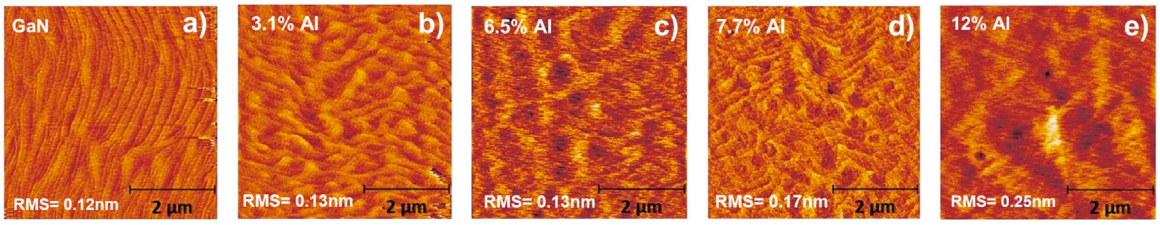

Fig. 1. 5 × 5 μm² AFM images of n-GaN layer (a) and n-$Al_xGa_{1-x}N$ layers with Al compositions of 3.1% (b), 6.5% (c), 7.7% (d) and 12% (e).

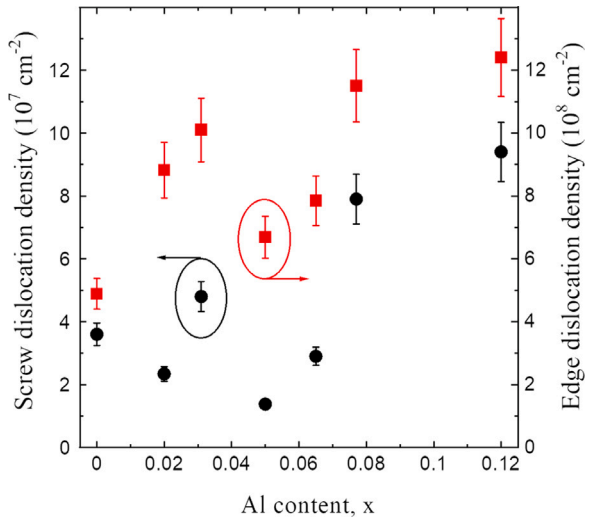

Fig. 2. Screw and edge dislocation densities versus the Al content, x, in the n-$Al_xGa_{1-x}N$ layers.

then increase for $x = 0.077$ and above. Note that the increase in screw dislocation density in the n-$Al_{0.12}Ga_{0.88}N$ layer may explain the higher RMS observed (Fig. 1(e)).

Representative reciprocal space maps (RSMs) around the $10\bar{1}5$ reciprocal space point for GaN and $Al_xGa_{1-x}N$ layers with $x = 0.02$, 0.05 and 0.12 are shown on Fig. 3. The RSMs have the elliptical shape typical for III-nitrides with a mosaic structure. The RSM broadening directions of the GaN layer and the $Al_xGa_{1-x}N$ layer with $x = 0.02$ are parallel and perpendicular to the surface. It can be seen that the RSM broadening direction for the $Al_{0.05}Ga_{0.95}N$ is somewhat inclined to the lateral direction (‖ to the surface) towards the direction perpendicular to the Q-vector (ω-direction), which indicates increase in mosaic tilt and a decrease in lateral domain size. The RSM inclination is more pronounced for the layer with Al-content of 12% (Fig. 3). These results are consistent with the observed increase in screw type dislocations for the layers with higher Al-content (Fig. 2).

In addition, a relatively high in-plane compressive strain of −0.046 was estimated for the GaN layer from the respective RSM. This result is in agreement with previous works on GaN layers with thickness below 1 μm grown on AlN/6H-SiC [23]. The compressive in-plane strain was attributed to the fact that initially GaN grows coherently on the AlN buffer layer. Even though, beyond a critical thickness of few nanometers the compressive strain starts to be partially relieved, full relaxation is not achieved for our 700 nm-thick layer. This long-range relaxation was associated with the difficulty of threading dislocations in the group III-nitrides to bend over and glide in the c-plane [24]. The tensile strain, induced as a consequence of the different thermal expansion coefficient of GaN and the SiC substrate, is not sufficient to compensate the remaining compressive strain due to the lattice mismatch. In contrast, for the $Al_xGa_{1-x}N$ layer with $x = 0.12$ the in-plane strain estimated from the respective RSM is slightly tensile and has a value of 0.001. This can be understood in view of a lower compressive strain due to the lattice mismatch between the AlN buffer layer and the $Al_xGa_{1-x}N$ as compared to the case of GaN. Consequently, the thermally induced tensile strain overcomes the lattice-mismatched induced compression.

3.2. Impurity incorporation

A multilayer structure with Si-doped $Al_xGa_{1-x}N$ layers with different Al content was used for the investigation of impurity incorporation (Fig. 4(a)). This structure was grown at a constant SiH_4 flow and a constant growth temperature, only the TMAl flow was varied. The SIMS depth profile of the multilayer structure is shown in Fig. 4(b). We note that the Al content obtained by SIMS for the individual layers in the stack agrees very well with that determined from XRD measurements on single $Al_xGa_{1-x}N$ layers with the corresponding growth conditions. The SIMS results in Fig. 4(b) show that Si, C, O and H concentrations remain constant in all $Al_xGa_{1-x}N$ layers in the stack, i.e. up to $x = 0.077$. The slightly lower [Si] in $Al_{0.031}Ga_{0.969}N$ close to the layer/substrate interface is probably due to the ramping down of the growth temperature. Importantly, the C level is below 2×10^{16} cm^{-3} for all Al compositions up to $x = 0.077$ and which is comparable to that obtained previously for epitaxial GaN grown on SiC by hot-wall MOCVD [17,25]. Carbon atoms introduced from the metalorganic sources during MOCVD growth occupy the N site in n-type GaN (C_N) and are a major source of compensating acceptors. C_N interferes with the precise control of free electron concentration of the n-type drift layer and affects negatively the blocking voltage and other device characteristics. Therefore, keeping [C] at the levels in GaN indicates goods prospects of using $Al_xGa_{1-x}N$ layers with Al content up to $x = 0.077$ in power devices.

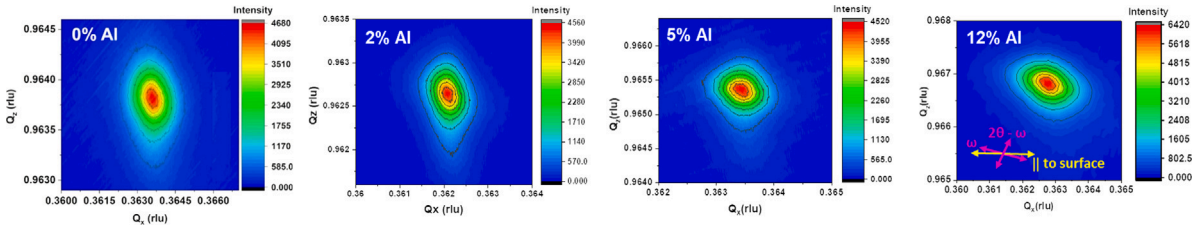

Fig. 3. Representative RSMs around the GaN 10$\bar{1}$5 reciprocal lattice point for the n-$Al_xGa_{1-x}N$ layers with x = 0, 0.02, 0.05 and 0.12. The ω and $2\theta-\omega$ scan directions, and the direction parallel to the sample surface are indicated in the RSM of $Al_{0.12}Ga_{0.88}N$ layer (same for all RSMs).

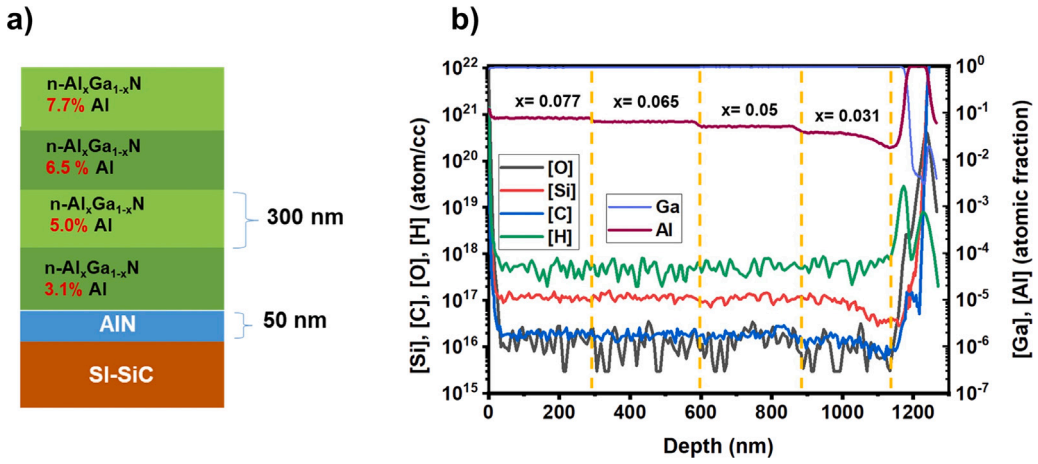

Fig. 4. (a) A schematic of the epitaxial multilayer structure used for SIMS, (b) Impurity concentrations as a function of layer depth in n-$Al_xGa_{1-x}N$ layers controlled by different TMAl flows.

The low C concentration could be further inferred from the CL spectra of the $Al_xGa_{1-x}N$ layers shown in Fig. 5. There is almost no trace of yellow luminescence (YL) except for the $Al_{0.12}Ga_{0.88}N$ layer. We note that the YL in n-$Al_xGa_{1-x}N$ is attributed to the presence of the C_N acceptors [26]. The CL spectra are dominated by the near-bang edge emission which for these particular layers arises from the free-exciton recombination. Accounting for the exciton binding energy, the peak energy positions in the spectra correspond very well with the bandgap energies obtained from SE and summarized in Table 1.

3.3. Electrical properties

The net donor concentration ($N_D - N_A$) in the n-$Al_xGa_{1-x}N$ layers obtained from C-V measurements are listed in Table 1. The measurements rely on determination of the capacitance (C) in the depletion region below a small area Schottky contact. A reverse DC voltage (V) superimposed with a small-signal AC voltage with a frequency of 10 Hz was applied. From the charge neutrality equation for the depletion region one can obtain [27]

$$N_D - N_A = \frac{2}{q\epsilon A^2 d(C^2)/dV} \tag{3}$$

where q is the electron charge, ϵ is the dielectric constant, and A is the diode area.

The measured capacitance as a function of the DC voltage for the n-$Al_xGa_{1-x}N$ layers is shown in Fig. 6. The obtained linear dependences of $1/C^2$ on the voltage indicate an uniform doping distribution in the depletion region. Then $N_D - N_A$ was calculated from the slope ($d(C^2)/dV$) using the dielectric constant of GaN for all layers. As seen from Table 1, the $N_D - N_A$ correlates with Si doping concentration for n-GaN and n-$Al_{0.031}Ga_{0.969}N$ layers. The deviation observed for higher Al contents can be attributed to the presence of compensating acceptors different from C_N. The free electron concentration measured by Hall effect in all studied layers is slightly lower than $N_D - N_A$ (see Table 1).

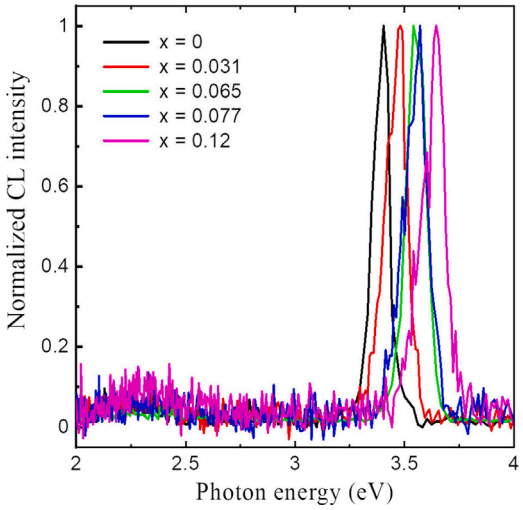

Fig. 5. Representative room-temperature CL spectra of n-$Al_xGa_{1-x}N$ layers.

This is commonly observed in n-GaN heteroepitaxial layers and can be explained by the trapping of electrons at dislocations.

The mobility measured in the n-GaN layer is comparable to the reported values for heteroepitaxial MOCVD GaN material with similar free electron concentrations [28]. With increasing Al content up to x = 0.077 the mobility gradually decreases. However, the decrease is not monotonic as one could expect considering that electron-alloy scattering is enhanced with increasing Al content. On the other hand, the measured mobility values were found to anti-correlate with the dislocation density (see Table 1). Hence, we can conclude that at very low Al contents the mobility is limited by electron-dislocation scattering rather than by electron-alloy scattering. For n-$Al_{0.12}Ga_{0.88}N$

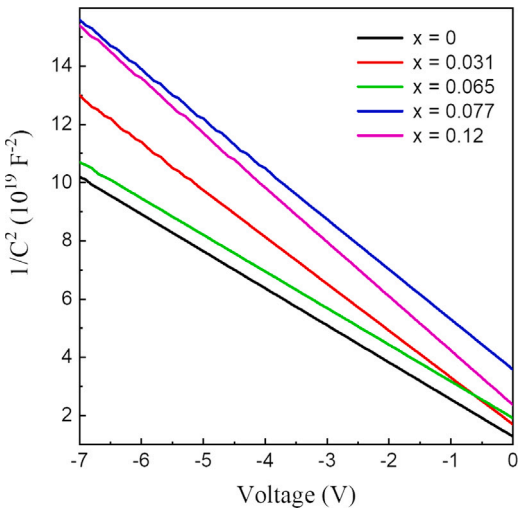

Fig. 6. Representative $1/C^2$ vs V plots for the n-$Al_xGa_{1-x}N$ layers. The slop was used to calculate the net donor concentration ($N_D - N_A$).

layer, the mobility drops significantly indicating that the electron-alloy scattering becomes significant for this Al content.

The critical electric field estimated following Ref. [3] and the BFOM for unipolar devices, estimated following Ref. [4] are shown in Table 1 for all layers. Due to the bandgap energy increase with Al content the respective E_c slightly increases with x. The BFOM is calculated using the measured mobility in the layers and normalized to the BFOM estimated for the reference GaN layer. Despite of the lower mobility in the n-$Al_xGa_{1-x}N$ layers, BFOM remains close to that of n-GaN up to $x = 0.077$. By reducing the dislocation density, i.e. using thicker Al(Ga)N buffer layers or/and GaN substrates, and thus increasing the mobility, we can expect to enhance BFOM in n-$Al_xGa_{1-x}N$ ($x < 0.08$) by at least 10%. We note that the higher E_c and enhanced BFOM would enable larger breakdown voltage ratings for the same n-type doping and thickness as compared to GaN.

4. Conclusions

In this study, we have investigated the defect density, impurity concentrations and electrical properties of low-Al-content n-$Al_xGa_{1-x}N$ layers in view of their potential to be employed as drift layers in vertical power devices. The 700-nm-thick crack-free Si-doped $Al_xGa_{1-x}N$ layers ($x = 0-0.12$) with smooth surfaces have been grown on 4H-SiC substrates by hot-wall MOCVD. Edge type dislocations were found to gradually increase with the Al content while screw dislocations were only enhanced for x above 0.077. Importantly, the impurity concentrations and most notably [C] remain at similar low levels (below 2×10^{16} cm^{-3}) up to $x = 0.077$ as revealed by SIMS and CL spectroscopy. The electron mobility was found to decrease with Al content in anti-correlation with the dislocation densities. Nonetheless, they still remained relatively high with e.g., a value of 407 $cm^2/(V.s)$ for $Al_{0.077}Ga_{0.923}N$. Comparable BFOMs for the $Al_xGa_{1-x}N$ layers up to $x = 0.077$ were estimated using the respective experimentally determined mobility and bandgap energy. On the other hand, increase of Al content to 12% resulted in deteriorated crystal quality and electron mobility, and hence significantly lower BFOM. Based on our results we propose that decreasing dislocation densities in n-$Al_xGa_{1-x}N$ layers with $x = 0.05-0.08$ by, e.g. growth on GaN substrates, may provide a route to explore such drift layers in power device applications.

CRediT authorship contribution statement

Vallery Stanishev: Writing – review & editing, Investigation, Formal analysis, Data curation. **Nerijus Armakavicius:** Writing – review & editing, Investigation, Formal analysis, Data curation. **Daniela Gogova:** Writing – review & editing, Supervision. **Muhammad Nawaz:** Writing – review & editing, Supervision. **Niklas Rorsman:** Writing – review & editing, Investigation, Formal analysis, Data curation. **Plamen P. Paskov:** Writing – review & editing, Supervision, Investigation. **Vanya Darakchieva:** Writing – original draft, Supervision, Resources, Project administration, Methodology, Investigation, Funding acquisition, Conceptualization.

Declaration of competing interest

The authors declare no conflict of interest.

Data availability

Data will be made available on request.

Acknowledgments

This work is performed within the framework of the Center for III-Nitride Technology (C3NiT-Janzén) supported by the Swedish Governmental Agency for Innovation Systems (VINNOVA) under the Competence Center Program Grant No. 2022-03139 with Lund University, Linköping University, Chalmers University of Technology, Hitachi Energy, Ericsson, Epiluvac, FMV, Gotmic, Region Skåne, Saab, SweGaN, Volvo Cars and UMS. We further acknowledge the support by the Swedish Research Council VR under Award No. 2016-00889 and 2022-04812, Swedish Foundation for Strategic Research under Grants No. EM16-0024 and STP19-0008, and the Swedish Government Strategic Research Area in Materials Science on Functional Materials at Linköping University, Faculty Grant SFO Mat LiU No. 2009-00971. We acknowledge Rosalia Delgado Carrascon and Son Puong Le.

References

[1] F. Iacopi, M.V. Hove, M. Charles, K. Endo, Power electronics with wide bandgap materials: Toward greener, more efficient technologies, MRS Bull. 40 (2015) 390.
[2] J.Y. Tsao, S. Chowdhury, M.A. Hollis, D. Jena, N.M. Johnson, K.A. Jones, R.J. Kaplar, S. Rajan, C.G. Van de Walle, E. Bellotti, C.L. Chua, R. Collazo, M.E. Coltrin, J.A. Cooper, K.R. Evans, S. Graham, T.A. Grotjohn, E.R. Heller, M. Higashiwaki, M.S. Islam, P.W. Juodawlkis, M.A. Khan, A.D. Koehler, J.H. Leach, U.K. Mishra, R.J. Nemanich, R.C.N. Pilawa-Podgurski, J.B. Shealy, Z. Sitar, M.J. Tadjer, A.F. Witulski, M. Wraback, J.A. Simmons, Ultrawide-bandgap semiconductors: Research opportunities and challenges, Adv. Electron. Mater. 4 (2018) 1600501.
[3] J.L. Hudgins, G.S. Simin, E. Santi, M.A. Khan, An assessment of wide bandgap semiconductors, IEEE Trans. Power Electron. 18 (2003) 907.
[4] B.J. Baliga, Gallium nitride devices for power electronic applications, Semicond. Sci. Technol. 28 (2013) 074011.
[5] D.Q. Tran, R.D. Carrascon, M. Iwaya, B. Monemar, V. Darakchieva, P.P. Paskov, Thermal conductivity of $Al_xGa_{1-x}N$ ($0 \le x \le 1$) epitaxial layers, Phys. Rev. Mater. 6 (2022) 104602.
[6] S. Keller, S.P. DenBaars, Metalorganic chemical vapor deposition of group III nitrides - a discussion of critical issues, J. Cryst. Growth 248 (2003) 479.
[7] H. Morkoc, Handbook of nitride semiconductors and devices, in: Materials Properties, Physics and Growth, Vol. 1, Wiley-VCH, Weinheim, 2008.
[8] S. Keller, G. Parish, P.T. Fini, S. Heikman, C.-H. Chen, N. Zhang, S.P. DenBaars, U.K. Mishra, Y.-F. Wu, Metalorganic chemical vapor deposition of high mobility AlGaN/GaN heterostructures, J. Appl. Phys. 86 (1999) 5850.
[9] K. Ikenaga, A. Mishima, Y. Yano, T. Tabuchi, K. Matsumoto, Growth of silicon-doped $Al_{0.6}Ga_{0.4}N$ with low carbon concentration at high growth rate using high-flow-rate metal organic vapor phase epitaxy reactor, Japan. J. Appl. Phys. 55 (2016) 05FE04.
[10] Y. Taniyasu, M. Kasu, N. Kobayashi, Intentional control of n-type conduction for Si-doped AlN and $Al_xGa_{1-x}N$ ($0.42 \le x < 1$), Appl. Phys. Lett. 81 (2002) 1255.
[11] A. Kakanakova-Georgieva, U. Forsberg, I. Ivanov, E. Janzén, Uniform hot-wall MOCVD epitaxial growth of 2-inch AlGaN/GaN HEMT structures, J. Cryst. Growth 300 (2007) 100.

[12] D. Gogova, M. Ghezellou, D.Q. Tran, S. Richter, A. Papamichail, J. ul Hassan, A.R. Persson, P.O.Å. Persson, O. Kordina, B. Monemar, M. Hilfiker, M. Schubert, P.P. Paskov, V. Darakchieva, Epitaxial growth of β-Ga_2O_3 by hot-wall MOCVD, AIP Adv. 12 (2022) 055022.

[13] H. Zhang, P.P. Paskov, O. Kordina, J.-T. Chen, V. Darakchieva, N-polar aln nucleation layers grown by hot-wall mocvd on sic: Effects of substrate orientation on the polarity, surface morphology and crystal quality, Physica B 580 (2020) 411819.

[14] S. Schöche, T. Hofmann, D. Nilsson, A. Kakanakova-Georgieva, E. Janzén, P. Kühne, K. Lorenz, M. Schubert, V. Darakchieva, Infrared dielectric functions, phonon modes, and free-charge carrier properties of high-Al-content $Al_xGa_{1x}N$ alloys determined by mid infrared spectroscopic ellipsometry and optical Hall effect, J. Appl. Phys. 121 (2017) 205701.

[15] H. Zhang, J.-T. Chen, A. Papamichail, I. Persson, P.P. Paskov, V. Darakchieva, High-quality N-polar GaN optimization by multi-step temperature growth process, J. Cryst. Growth 603 (2023) 127002.

[16] H. Zhang, I. Persson, J.-T. Chen, A. Papamichail, D.Q. Tran, P.O. ÃČ Persson, P.P. Paskov, V. Darakchieva, Polarity control by inversion domain suppression in N-polar III-nitride heterostructures, Cryst. Growth Des. 23 (2023) 1049–1056.

[17] A. Papamichail, A. Kakanakova-Georgieva, E.Ö. Sveinbjörnsson, A.R. Persson, B. Hult, N. Rorsman, V. Stanishev, S.P. Le, P.O.Å. Persson, M. Nawaz, J.T. Chen, P.P. Paskov, V. Darakchieva, Mg-doping and free-hole properties of hot-wall MOCVD GaN, J. Appl. Phys. 131 (2022) 185704.

[18] R. Delgado Carrascon, S. Richter, M. Nawaz, P.P. Paskov, V. Darakchieva, Hot-wall MOCVD for high-quality homoepitaxy of GaN: Understanding nucleation and design of growth strategies, Cryst. Growth Des. 22 (2022) 7021.

[19] V. Darakchieva, B. Monemar, A. Usui, On the lattice parameters of GaN, Appl. Phys. Lett. 91 (2007) 031911.

[20] R. Delgado Carrascon, D.Q. Tran, P. Sukkaew, A. Mock, R. Ciechonski, J. Ohlsson, Y. Zhu, O. Hultin, B. Monemar, P.P. Paskov, L. Samuelson, V. Darakchieva, Optimization of GaN nanowires reformation process by metalorganic chemical vapor deposition for device-quality GaN templates, Phys. Status Solidi b 257 (2020) 1900581.

[21] T. Metzger, R. Höpler, E. Born, O. Ambacher, M. Stutzmann, R. Stömmer, M. Schuster, H. Göbel, S. Christiansen, M. Albrecht, H.P. Strunk, Defect structure of epitaxial gan films determined by transmission electron microscopy and triple-axis x-ray diffractometry, Phil. Mag. A 77 (1998) 1013.

[22] V. Srikant, J.S. Speck, D.R.K. Clarke, Mosaic structure in epitaxial thin films having large lattice mismatch, J. Appl. Phys. 82 (1997) 4286.

[23] S. Einfeldt, Z. Reitmeier, R. Davis, Surface morphology and strain of GaN layers grown using 6H-SiC(0001) substrates with different buffer layers, J. Cryst. Growth 253 (2003) 129.

[24] B. Jahnen, M. Albrecht, W. Dorsch, S. Christiansen, H.P. Strunk, D. Hanser, R.F. Davis, Correlation between mobility collapse and carbon impurities in Si-doped GaN grown by low pressure metalorganic chemical vapor deposition, MRS Internet J. Nitride Semicond. Res. 3 (1998) 39.

[25] J.-T. Chen, U. Forsberg, E. Janzén, Impact of residual carbon on two-dimensional electron gas properties in $Al_xGa_{1-x}N$/GaN heterostructure, Appl. Phys. Lett. 102 (2013) 193506.

[26] P.P. Paskov, B. Monemar, in: W. Bi, P.C. Ku, H.C. Kuo, B. Shen (Eds.), Handbook of GaN Semiconductor Materials and Devices, Taylor and Francis, 2017, p. 87.

[27] D.K. Schroder, Semiconductor Material and Device Characterization, third ed., Wiley, 2006, pp. 61–79.

[28] F. Kaess, S. Mita, J. Xie, P. Reddy, A. Klump, L.H. Hernandez-Balderrama, S. Washiyama, A. Franke, R. Kirste, A. Hoffmann, R. Collazo, Z. Sitar, Correlation between mobility collapse and carbon impurities in Si-doped GaN grown by low pressure metalorganic chemical vapor deposition, J. Appl. Phys. 120 (2016) 105701.